International Journal of Impact Engineering 36 (2009) 165–176

Contents lists available at ScienceDirect

International Journal of Impact Engineering

journal homepage: www.elsevier.com/locate/ijimpeng

Dynamic crushing of honeycombs and features of shock fronts

Z. Zou [a,*], S.R. Reid [b], P.J. Tan [c], S. Li [a], J.J. Harrigan [b]

[a] School of Mechanical, Aerospace and Civil Engineering, The University of Manchester, Pariser Building, P.O. Box 88, Sackville Street, Manchester M60 1QD, UK
[b] Department of Engineering, University of Aberdeen, Fraser Noble Building, King's College, Aberdeen AB24 3UE, UK
[c] Department of Mechanical Engineering, UCL, Torrington Place, London WC1E 7JE, UK

ARTICLE INFO

Article history:
Received 5 June 2007
Received in revised form 18 November 2007
Accepted 19 November 2007
Available online 22 May 2008

Keywords:
Honeycombs
Shock
Impact
Finite elements

ABSTRACT

The in-plane dynamic crushing of 2D hexagonal-cell honeycombs has been simulated using finite elements to explore the dynamic response of cellular materials and to investigate the features of the crushing front and to examine the assumptions employed in a one-dimensional shock theory [Reid SR, Peng C. Dynamic uniaxial crushing of wood. Int J Impact Eng 1997;19:531–70; Tan PJ, Reid SR, Harrigan JJ, Zou Z, Li S. Dynamic compressive strength properties of aluminium foams. Part II – shock theory and comparison with experimental data and numerical models. J Mech Phys Solids 2005;53:2206–30]. It has been demonstrated that progressive cell crushing is observed to propagate through the material in a 'shock' like manner when the crushing velocity exceeds a critical value. The simulations show that there exists a zone at the shock front across which there are essentially discontinuities in the material 'particle velocity', 'stress' and 'strain' as defined herein. At supercritical crushing velocities the thickness of this zone remains about one cell size, which varies little with the crushing velocity and the relative density. Densification strain increases as crushing velocity increases and asymptotes to a limit once a shock front forms. It has also been shown that the one-dimensional shock theory [Reid SR, Peng C. Dynamic uniaxial crushing of wood. Int J Impact Eng 1997;19:531–70; Tan PJ, Reid SR, Harrigan JJ, Zou Z, Li S. Dynamic compressive strength properties of aluminium foams. Part II – shock theory and comparison with experimental data and numerical models. J Mech Phys Solids 2005;53:2206–30], which was based on an equivalent rigid-perfectly plastic-locking stress–strain curve, tends to overestimate slightly the crushing stress and energy absorbed.

1. Introduction

Honeycombs, foams and other cellular materials have been proposed for use in impact energy absorption and shock mitigation applications. Extensive theoretical and experimental work has been carried out on cellular materials under quasi-static and dynamic loading. Some of the results of the former were summarised comprehensively in Gibson and Ashby [3] and the dynamic/impact behaviour was reviewed by Reid et al. [4].

In quasi-static crushing of cellular materials, individual cells can exhibit a wide spectrum of behaviour resulting from the elastic deformation, buckling and plastic collapse of the cell walls. The deformations in separate cells tend to interact with each other resulting in complex patterns of deformation. Localisation is a characteristic feature of the compression behaviour of cellular materials. Collapse takes place at the weakest row or band of cells first and gradually spreads to stronger areas of the structure. The process produces a nominal stress–strain curve which, overall, is convex towards the strain axis in the post-yield (plateau) and densification régimes.

Crushing of a cellular material under impact (suddenly imposed boundary velocity) conditions is quite different from its quasi-static counterpart, the crushing behaviour being dominated by structural and dynamic/inertial effects for moderate impact velocities and by stress wave propagation under relatively high impact velocities. One of the most distinctive features is that enhanced stress levels are required to crush the material. The initial peak impact loads and plateau loads all increase with increasing impact velocity. From experimental data, Reid and Peng [1] reported enhanced crushing strength for wood under dynamic conditions. Zhao and Gary [5] found a significant enhancement in the out-of-plane crushing force in aluminium honeycombs through an experimental investigation. Aluminium foam showed a similar tendency under dynamic conditions as reported by Tan et al. [6,7]. An increase was also exhibited in the impact energy absorption capacity of the cellular material over that measured in a quasi-static test. Hönig and Stronge [8,9] illustrated a strong increase of the total dissipated energy for 2D honeycombs with increasing impact velocity through finite element simulations.

* Corresponding author. Tel.: +44 161 3062403.
E-mail address: z.zou@manchester.ac.uk (Z. Zou).

0734-743X/$ – see front matter © 2008 Elsevier Ltd. All rights reserved.
doi:10.1016/j.ijimpeng.2007.11.008

Dynamic crushing of cellular materials involves deformation patterns that are even more localised than those in a quasi-static process. When the impact velocity is high enough, a crushing front forms at the impact end and propagates through the cellular structure. Whilst the cells behind the crushing front are fully crushed (i.e. a state of deformation where no further deformation is possible until the complete length of the honeycomb has been crushed), those ahead of the crushing front remain almost undeformed. This deformation pattern is reminiscent of a propagating shock [7].

There is now an extensive literature on 'shock propagation' in cellular systems and the dynamic enhancement of crushing strengths with impact velocity has been correlated using a simple shock theory. A 'structural' shock model for ring systems was first proposed by Reid et al. [10]. To provide a first order understanding of the dynamic response, a simple one-dimensional shock model based upon a rate-independent, rigid-perfectly plastic-locking (*R-P-P-L*) idealisation of a representative stress–strain relationship for wood was developed by Reid and Peng [1]. This predicted well the stress associated with the propagation of the crushing process. This theory showed that the crushing stress was proportional to the square of the impact velocity and the predictions using the theory compared well with experimental data, particularly for crushing across the grain of the wood. This model has been presented recently in a more extensive thermo-mechanical treatment for metallic foams by Tan et al. [2].

The simple *R-P-P-L* estimate of the shock-induced stress enhancement in a cellular material has been employed in various publications to assess the significance of the dynamic stresses in cellular materials [6,11,12]. The shock theory has also been extended by Lopatnikov et al. [13,14] to include the effect of elasticity and an elastic-perfectly plastic-rigid (*E-P-P-R*) model was proposed. Based on rigid-softening-hardening and elastic-softening-hardening material models, the shock theory was recently used to analyse the dynamic crushing of wood along the grain direction by Harrigan et al. [15].

Whilst 3D models remain to be developed, finite element analysis has been usefully employed to investigate the dynamic crushing of 2D structures/material in the literature. Ruan et al. [16] studied the in-plane dynamic crushing of regular honeycombs. Three different 'patterns' of deformation, viz. '*X*', '*V*' and '*I*', were identified for different compression rates. Zheng et al. [17] further investigated the behaviour of 2D irregular cellular structures. The velocities for transition between deformation patterns were identified and expressed by (numerically) empirical equations. The deformation pattern '*I*' in these two papers corresponds to the stage when a shock-type front forms and propagates through the cellular structure.

Finite element analysis was also employed in the work reported herein to simulate the in-plane, constant velocity, uniaxial dynamic crushing of regular, and hexagonal honeycombs. Long honeycombs have been considered to minimise boundary effects from the two ends. The crushing behaviour was examined over a range of compression speeds up to 200 m/s.

In many cellular material papers, continuum terminology is used but the finite cell dimensions need to be recognised. Therefore, in this paper, particular attention has been given to defining appropriate local engineering strain and stress averaged over selected cross-sections and examining their distributions throughout the honeycomb during the crushing process. The aim of this study is to understand better the characteristics of 'structural shocks' in cellular materials. These characteristics include the discontinuities (sharp jumps) in stresses and strains across the shock front and the thickness of the shock itself. Furthermore, the numerical predictions are compared with the shock theory developed in the literature [1,2], in order to test that theory and the assumptions on which it is based.

2. One-dimensional shock theory

Using conventional continuum mechanics definitions of axial stress and specimen strain, beyond the elastic range the quasi-static nominal stress–strain curves for cellular materials are generally convex towards the strain axis, and, according to non-linear wave theory, shocks are therefore expected to form under dynamic loading. Thus, when a cellular material is crushed at a sufficiently high velocity, it might be expected that a structural shock is generated and propagates through the cellular material. Following this conjecture, to estimate the enhancement in the crushing stress as a function of impact speed, Reid and his co-authors [1,2,6] developed a simple one-dimensional 'shock' model. The representation of the nominal stress–strain curve of a typical cellular material was simplified to the rigid-perfectly plastic-locking (*R-P-P-L*) idealisation shown in Fig. 1a. The material locks at a locking strain ε_d (densification strain). In the simple theory, when the cellular material rod shown in Fig. 1b is crushed by a moving rigid mass *M*, because of the rigid nature of the initial response, it is assumed that the stress in the material particle ahead of the shock front is instantaneously raised to the quasi-static crushing strength σ_0 as in classical rigid-plastic wave theory. As the shock passes through the material, it increases the material particle velocity to that of the striker, increases the density of the material by compaction up to the locking strain ε_d (assumed independent of impact velocity in Ref. [2]) and raises the stress to a value σ. Therefore there are discontinuities in material particle velocity, stress and strain across the 'shock' front. The equations governing the propagation of the shock are made up of kinematical equations and equations of conservation of mass and momentum for the material crossing the shock front. The dynamic crushing stress at the proximal end was derived as in Refs. [1,2,6]

$$\sigma = \sigma_0 + \frac{\rho V^2}{\varepsilon_d}, \tag{1}$$

where ρ is the initial density of the cellular material and *V* is the velocity of the striker. This equation provides an estimate of the crushing stress at a given impact velocity *V*. The shock model can also be used to calculate the variation in σ with time [1]. For the

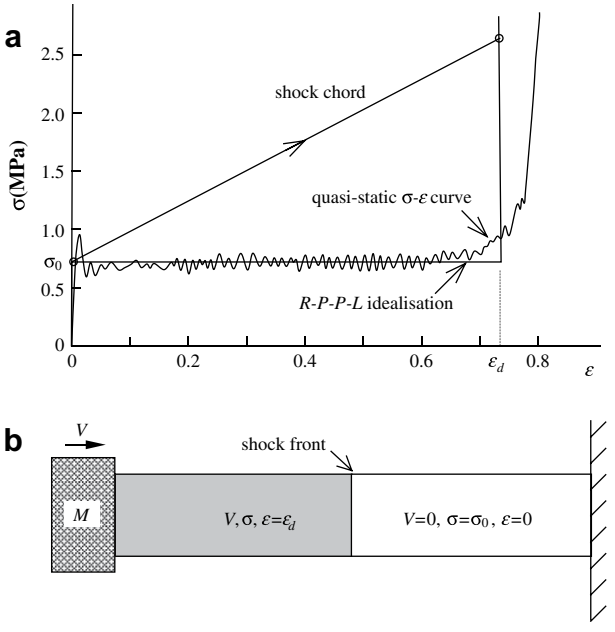

Fig. 1. Shock wave model: (a) idealised *R-P-P-L* stress–strain curve; (b) basic parameters.

simpler problem of compression at a constant velocity, the above crushing stress is a constant with time and equal to the dynamic plateau stress σ_{pl} as defined in Tan et al. [6].

In the *R-P-P-L* shock theory, the stress and strain traverse the shock chord [2] joining the conditions ahead of and behind the shock front instead of the quasi-static stress–strain curve as shown in Fig. 1a. The specific plastic energy dissipation is given by

$$E_p = \frac{1}{2}(\sigma + \sigma_0)\varepsilon_d = \sigma_0\varepsilon_d + \frac{1}{2}\rho V^2. \quad (2)$$

Eqs. (1) and (2) both show a quadratic variation of the dynamic crushing stress and plastic energy with crushing velocity.

3. Impact velocity régimes

Using continuum models for the material, the response of cellular materials when struck by a rigid mass can be classified according to the impact velocity, wherein the boundaries to the different velocity régimes are a function of the stress–strain curve that represents the macroscopic material behaviour (see Refs. [13,14]). Within different velocity régimes, different waves are generated at the proximal end on impact. Using the *R-P-P-L* idealisation this classification is not possible. However, for a linear-elastic, perfectly plastic, locking material (*E-P-P-L*), the lowest velocity that governs a change in material response to the impact is that associated with the formation of a plastic wave upon impact, i.e.

$$V_y = \frac{\sigma_0}{\sqrt{\rho E}}, \quad (3)$$

where E is the elastic modulus of the cellular material. However, cellular materials have non-linear stress–strain behaviour at low strains (see Fig. 1). Hönig and Stronge [8] therefore used the "wave-trapping" speed to define the impact speed at which cell collapse will begin at cells adjacent to the impact mass. The wave trapping speed is given by

$$V_w = \int_0^{\varepsilon_w} c(\varepsilon)\mathrm{d}\varepsilon. \quad (4)$$

where ε_w is the strain when the stress is at its first peak and the gradient of the tangent modulus of the quasi-static stress strain curve is zero (so $c = 0$), and $c = \sqrt{\sigma'(\varepsilon)/\rho}$ and $\sigma'(\varepsilon) = \mathrm{d}\sigma/\mathrm{d}\varepsilon$.

At velocities greater than V_w, although cell collapse may be initiated in cells adjacent to the impact mass, complicated deformation patterns and kink bands can still be produced as the compression continues. With increasing impact velocity, the deformations become more localised until cell collapse occurs in a progressive manner from the proximal end. The cell collapse is governed by the progress of a "compaction wave" (similar to a plastic wave in a continuum) that travels through the cellular material in a shock-like manner. This has been termed a 'steady-shock' in Ref. [2]. The proposed kinematical condition for continuing 'steady-shock' wave propagation is discussed in Ref. [2]

$$V \geq V_s = \sqrt{2\sigma_0\varepsilon_d/\rho}. \quad (5)$$

The above expression gives the steady-shock velocity V_s beyond which progressive cell crushing exhibits 'shock' type (propagating discontinuity) characteristics. It is evident from Eq. (5) that this critical velocity depends on the quasi-static crushing strength, the locking strain and the density of the cellular material.

4. Finite element modelling and loading conditions

The finite element model analysed is shown in Fig. 2a corresponding to a rectangular sample comprises hexagonal cells. It is considered to be placed against a fixed rigid plate at one end (distal) and deformed by moving a rigid plate axially at a constant velocity V at the other end (proximal). The ends of the honeycombs are not tied to the two plates. Possible separations between the honeycomb sample and the rigid plates may occur during the crushing process. All the cells are identical, the length of the edges of the hexagonal cells being $l = 4$ mm. The model has been deliberately made long (about four times the width) to produce a steady state deformation pattern away from the ends. The cells were compressed in the X_1 direction as indicated in Fig. 2b in most cases, where the sample has 74 hexagonal cells along the loading direction (x) and 21 cells in the transverse direction (y). However, in order to examine any difference in the crushing behaviour, a few other cases were studied where cells were arranged with the X_2 direction aligned with the loading in x direction and there are 87 cells along x-direction and 19 cells in y direction in the sample. The cell wall material was assumed to be elastic, perfectly plastic with $E = 68$ GPa, $\sigma_y = 130$ MPa and $\rho_s = 2700\ \mathrm{kg\,m^{-3}}$. The numerical simulations are mainly based on a relative density $\overline{\rho} = \rho/\rho_s = 0.1$, which corresponded to a cell wall thickness of $t = \sqrt{3}l\overline{\rho}/2 = 0.346$ mm. The imposed crushing velocity was varied from 2 to 200 m/s in order to study the effects of the compression rate. ABAQUS/Explicit [18] was employed for the analyses.

Following collapse, deformation of the honeycomb cells involves extensive contacts between deformable cell walls. The pattern of cell collapse is non-symmetric and irregular in general. As a result, self-contact of the cell walls within each cell needs to be simulated. There is no capability in ABAQUS to simulate this type of contact between beam elements. However, ABAQUS does offer the option of self-contact surfaces for a class of shell elements. Consequently in this study, S4R (four-node doubly curved, reduced integration, hourglass controlled, finite membrane strain) shell elements were used. Only one layer of elements in the FE model was employed in the X_3 direction (perpendicular to the plane of the paper, see Fig. 2) with a depth of 4 mm. All the nodes were constrained in the X_3 direction to simulate a plane strain state in the x–y plane. Each of the six sides of the cell walls was modelled with four elements, which was proved to be sufficient to produce reliable results through a mesh sensitivity study. All possible contacts were considered during crushing, including self-contact within each cell and between the honeycomb and the end plates. No friction has been considered at the contact surfaces.

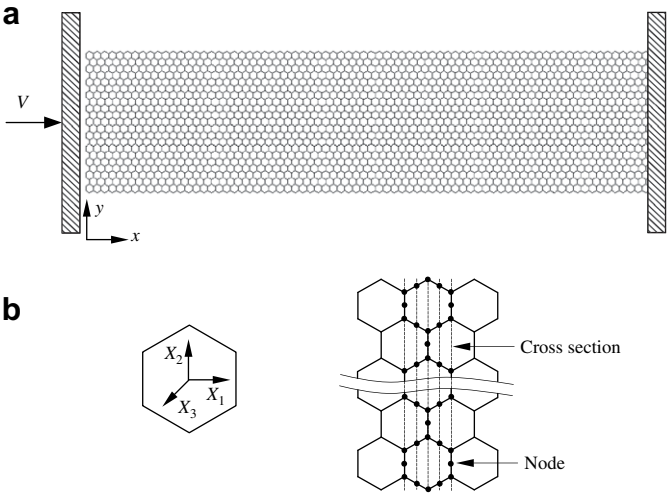

Fig. 2. (a) Honeycomb specimen and loading condition and (b) local directions for honeycomb and cross-sections for definition of key quantities.

The quasi-static nominal stress–strain curve of the honeycomb predicted by the FE analysis is given in Fig. 1 which was produced in the following manner. A static analysis was carried out using ABAQUS/Standard up to the initial peak where the analysis could not go any further due to the implicit algorithm employed. A separate analysis using ABAQUS/Explicit was also performed at a loading rate of 2 m/s. The initial part of the stress–compression curve was almost identical to the previous static analysis. The differences between the stresses obtained from the proximal and distal ends were insignificant. It is therefore reasonable to assume that the low velocity stress–compression curve represents its static counterpart. In this, there is an elastic rise to an initial peak followed by a stress drop and a subsequent nearly constant stress plateau. When all the cells are crushed, the stress increased drastically and the material undergoes a relatively small amount of deformation to compact the already densified honeycomb further at much high stresses.

To treat the long honeycomb conveniently as a one-dimensional continuum cellular rod and to evaluate the distributions of some key conventional quantities (such as cross-sectional displacement, particle velocity, stress and strain) along the rod during the crushing process, appropriate definitions for these quantities were introduced. These were used to interpret the results of the FE analysis. Cross-sectional values of these quantities were average values calculated from the 2D FE model and were used to overcome the complexity masking the gross behaviour over the width direction, y, of the honeycomb.

Along the loading direction x, sample cross-sections have been chosen in the undeformed honeycomb configuration in order to evaluate average displacements. The length of each cell in a given row is divided into four equal parts as shown in Fig. 2b. A cross-section is defined as the collection of the nodes on the plane of the cross-section. The cross-section moves as the cells are crushed. The displacements obtained from the FE analysis at all the nodes on a typical cross-section, such as that shown in Fig. 2b, were averaged to provide a displacement for that cross-section of the honeycomb. The average material 'particle' velocity for the cross-section can be defined in a similar way. Local engineering strain, ε, was then defined from the relative displacement between two neighbouring cross-sections. These strain measures are more suitable for high velocity impact where deformation propagates in layers perpendicular to the loading direction regardless of the structural dimensions rather than at lower impact velocities where there is variation across particular cross-sections.

Engineering stress, σ, was defined as the ratio between the total axial forces at the nodes on a cross-section and the sectional area. Hereafter, the particle velocity, strain and stress that are referred to in this paper are those defined above in the sense of cross-sectional values, not those for the cell wall material.

A non-dimensional global compression, δ, is defined as the ratio of the overall compression of the honeycomb and its original length and is employed to describe the extent of crushing of the honeycomb structure and is proportional to the crushing time since the honeycomb is compressed at a constant velocity.

Several criteria have been used in the literature to identify the plateau stress and densification strain. The one proposed by Tan et al. [6] was adopted statically and dynamically in this investigation, which is based on the energy absorption efficiency curve which gives unique and consistent results.

The use of a constant compression velocity in this study is to achieve a steady crushing process and to identify the characteristics of the crushing behaviour at a specific crushing velocity conveniently. It would be possible to simulate a realistic impact scenario, i.e. honeycombs impacted by a striker plate of large mass moving at a given initial velocity. As long as the mass is large enough, the reduction in the velocity of the striker would be insignificant as the kinetic energy gradually absorbed through plastic deformation of the honeycomb during the crushing process would be negligible. The assumption of constant crushing speed is considered acceptable in this paper as the focus is to capture the characteristics of the crushing behaviour *per se*.

5. Results and discussion

5.1. Dynamic crushing patterns and crushing stresses

Figs. 3–6 show deformation patterns under various crushing velocities, $V = 2$, 10, 50 and 100 m/s, respectively, when the cells were compressed in the X_1 direction. Each figure contains the deformation patterns at four typical crushing states in terms of the overall compression level, *viz.* $\delta = 0.05$, 0.20, 0.40 and 0.60. The load–displacement curve for $V = 2$ m/s has already been included in Fig. 1a as a close representation of its static counterpart. The load–displacement curves obtained at three higher crushing speeds are shown in Fig. 7 where the forces at proximal and distal ends are plotted. Based on the quasi-static stress strain curve in Fig. 1, the wave trapping velocity for the present honeycombs is $V_w = 6.4$ m/s according to Eq. (4) and $\varepsilon_w = 0.016$.

(i) When the honeycomb is crushed at a very low velocity ($V = 2$ m/s $< V_w$), cells collapse in an "X" pattern at the distal end first due to the interaction of the incident and reflected stress waves from the rigid end. This "X" shaped crushing pattern is apparently due to free edge effect from the sides. The cells near the two sides of the specimen have less lateral constraint than those near the centre. Deformation of the cells along a cross-section differs from each other due to the varying constraint across the cross-section, resulting in "X"

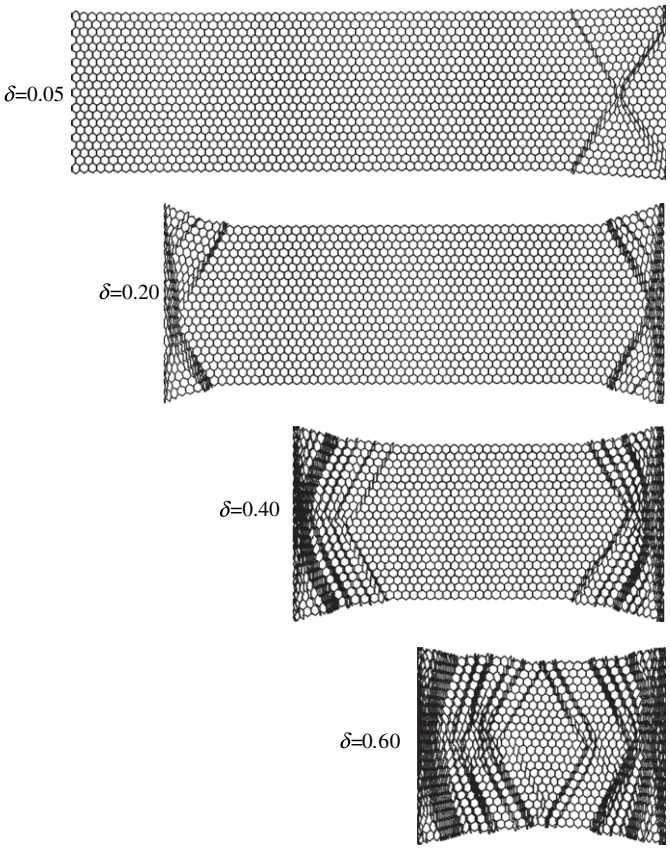

Fig. 3. Deformation process under compression velocity $V = 2$ m/s ($\bar{\rho} = 0.1$).

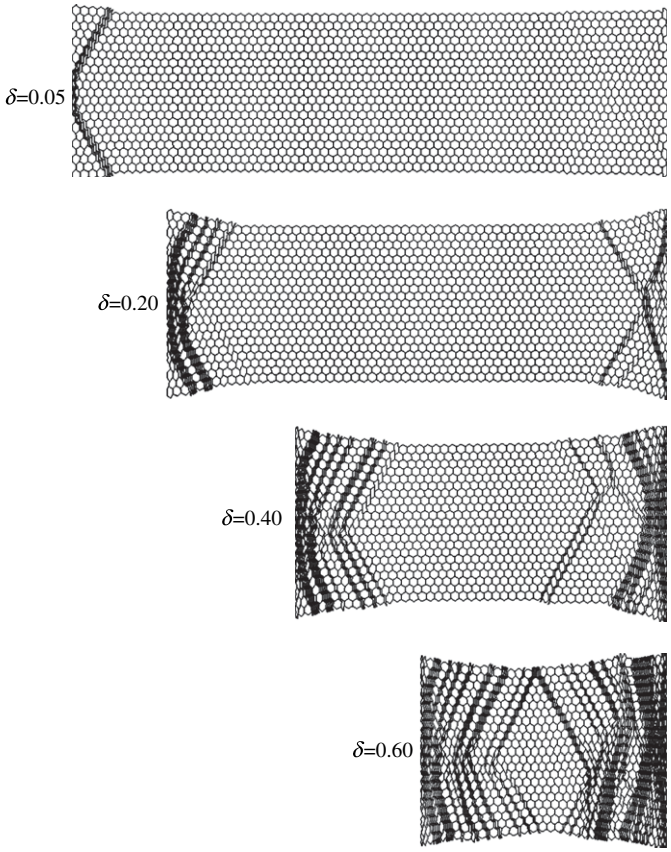

Fig. 4. Deformation process under compression velocity $V = 10$ m/s ($\bar{\rho} = 0.1$).

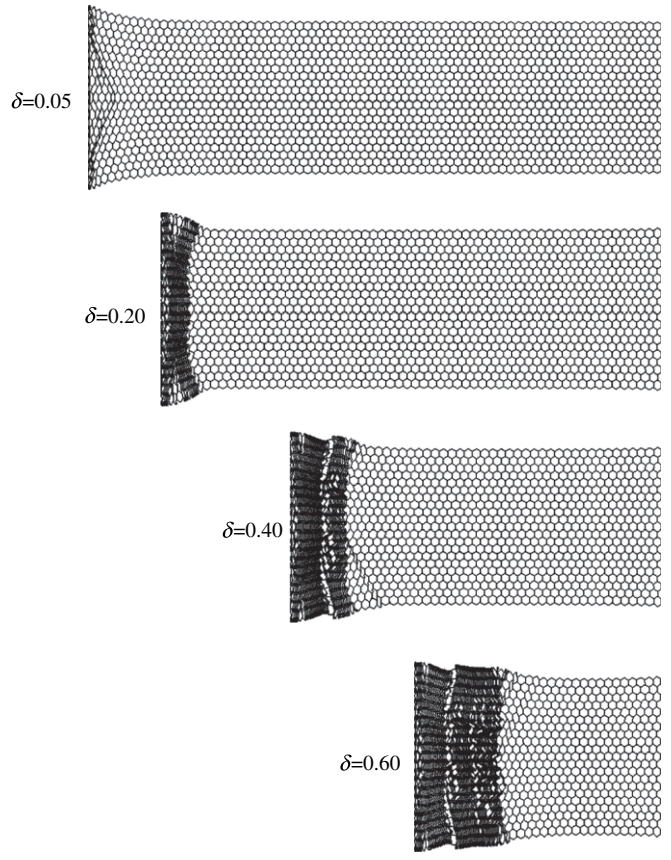

Fig. 5. Deformation process under compression velocity $V = 50$ m/s ($\bar{\rho} = 0.1$).

collapse band. As the overall compression continues to increase, cells start to collapse at the proximal end as well and gradually the crushing bands spread from both the distal and proximal ends to the middle of the honeycomb. The honeycomb deforms through cumulative multiplication of discrete crush bands.

(ii) Increase of the crushing velocity ($V = 10$ m/s $> V_w$) causes a "V" shaped crushing band to occur first at the proximal end. This is followed by an "X" shape at the distal end. This pattern is shown in Fig. 4 and can be explained in the same way as above with reference to wave fronts. As the velocity of the striker is greater than the wave trapping speed, cell collapse will be initiated in cells adjacent to the striker. The stress waves that are produced at the proximal end therefore contain both elastic and plastic components. In a similar manner to the propagation of elastic and plastic stress waves in a solid continuum that is struck at speeds greater than V_y, (Eq. 3), a precursor travels through the cellular solid followed by a larger magnitude wave that causes collapse of cells. The cellular nature of the material will, however, result in a more complicated deformation pattern than is the case for a solid continuum.

Additional runs of the finite element analysis indicate that the change of the pattern from the collapse of cells at the distal end to the collapse of cells at the proximal end occurs at impact speed between 6 m/s and 7 m/s, close to the wave trapping velocity $V_w = 6.4$ m/s predicted by Eq. (4). However, it has to be pointed out that collapse of cells still occurs at the distal end in later stages before the entire honeycomb is fully crushed, as shown in Fig. 4.

If the honeycomb had a length close to its width, as in Ruan et al. [16], multiple discrete crushing bands would not appear. Instead, two "X" shaped crushing bands would be expected at the proximal and distal ends, forming a rhombus at the middle of the honeycomb.

The deformation would also be different if there are imperfections in the honeycomb under low speed compression. Hönig and Stronge [8] examined the dynamic cell collapse mechanism with imperfections. Their simulations showed a crush band initiates at the impact surface when the impact velocity exceeds the wave trapping velocity, whilst below the wave trapping velocity the formation of the initial crush band was affected by the distribution and the extent of initial imperfections to a large extent.

(iii) Further increase in the crushing velocity results in collapse/crushing from the proximal end which propagates towards the distal end, as shown in Fig. 5 ($V = 50$ m/s). An interesting observation made during the analyses of the crushing processes under different speeds was that the initial peak stress on the quasi-static nominal stress strain curve was around 0.94 MPa, as shown in Fig. 1, which is very close to the proximal end plateau stress at the crushing speed of 30 m/s (results not shown here). Upon impact, the crushing stress is first generated at the proximal end and then transmitted to the distal end by stress waves. With increasing impact velocity the amplitude of the crushing stress now exceeds the peak stress in the quasi-static nominal stress strain curve. Hence, when the crushing speed exceeds 30 m/s, cell collapse starts from the proximal end only and gradually propagate towards the distal end as compression continues. The intensity of the stress waves that are transmitted to the cells adjacent to the distal end is not sufficient enough to crush them. It is difficult to understand how the collapse of cells at the distal end no longer occurs as impact velocities increase producing higher

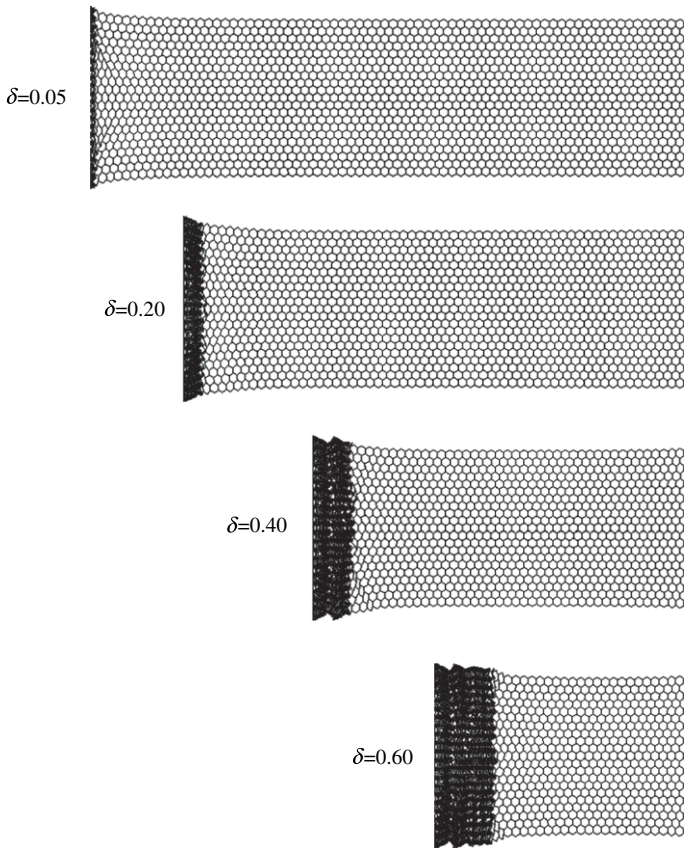

Fig. 6. Deformation process under compression velocity $V = 100$ m/s ($\bar{\rho} = 0.1$).

proximal end stresses. This phenomenon was noted experimentally in wood specimens [15], where the distal end loads increased (with increasing impact velocity) to a maximum at approximately $V = 60$ m/s then reduced gradually with impact velocity. This cannot be predicted using continuum wave theory for a linear-elastic, perfectly plastic, hardening material. However, it is a possible consequence of the non-linear material behaviour at small strains. For small strains, $\varepsilon < \varepsilon_w$, with increasing stress the waves travel with reduced speed so that it is possible that the waves associated with higher stresses but strains less than ε_w are caught up by the compaction wave. Additionally, it is possible that unloading waves caused by collapsing cells travel at higher speeds through the uncompacted region than the loading waves. In this way cells at the distal end may not be held at high enough stress over sufficiently long periods for them to collapse.

It is also observed that there is a regular series of compacted blocks from the proximal end with a block length of around 24 cell rows. There is no explanation for this at present.

(iv) When the loading velocity exceeds the steady-shock velocity, the crushing front propagates through the material in a shock-like manner, see $V = 100$ m/s. According to Eq. (5) the steady-shock velocity V_s is 66 m/s for the present honeycomb. For $V = 100$ m/s cells immediately ahead of the shock front are only slightly deformed and those away from the shock front are hardly deformed at all as shown in Fig. 6. The cells near the two sides of the specimen are less constrained than those near the centre. Under low compression velocity, deformation of the cells along a cross-section, in particular at the crushing front, differs from each other due to the varying constraint across the cross-section. However, when the compression velocity is sufficiently high, the lateral inertial forces are increased due to cell edge bending, resulting in a more similar constraint on most of the cells across a cross-section. The deformation across the cross-section becomes more uniform therefore, represented by an '*I*' shaped crushing front. Similar to the crush pattern at $V = 50$ m/s, there is a clearer, regular series of compacted blocks from the proximal end. The block length is, however, reduced to around 14 cell rows.

The deformation patterns of honeycomb cells compressed in the X_2 direction under different crushing velocities are similar to those crushed in X_1 direction, e.g. cells collapse at the distal end and proximal end first at low compression speeds and shocks form at high crushing speeds. The main difference is that the crushing bands are "*V*" and then "*I*" shaped at low compression speed instead of the "*X*" or "*V*" shapes. The collapse pattern has been analysed and discussed in Ref. [16]. However, some discussion is given below of the strain distribution.

The stresses produced at the proximal end at three crushing velocities, $V = 10$, 50 and 100 m/s are compared in Fig. 7a. All the curves show a long plateau with oscillations during the crushing process. The oscillation of stress is mainly caused by the self-contact within the collapsing cells, row by row, and the stress waves travelling in the compacted region. The type II crushing behaviour [19–21] in the collapse process of cells also contributes to the stress oscillations. As a feature of a type II behaviour, peak load increases with the crushing speed. As a result, more pronounced fluctuations are observed in the stress–compression curves for higher crushing speeds. An important trend in Fig. 7a is that the plateau stress at the proximal end increases with the crushing velocity. This has been reported and discussed extensively in the literature, e.g. see Refs. [1–6,16].

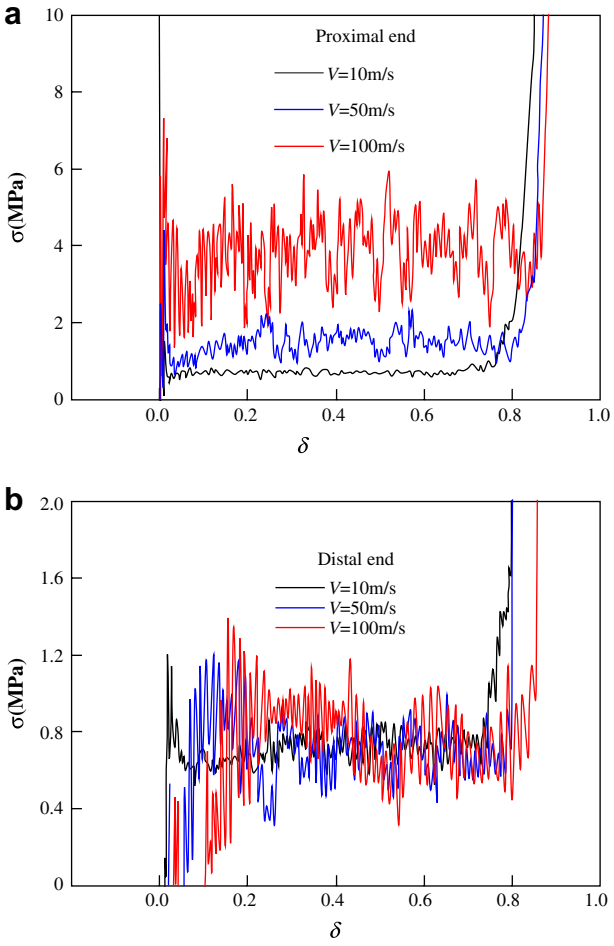

Fig. 7. History of stresses at the proximal and distal ends (cells compressed in X_1 direction, $\bar{\rho} = 0.1$).

In contrast to the crushing stress at the proximal end, crushing velocity has much less effect on the stress at the distal end over the entire crushing process, as shown in Fig. 7b. This is to be expected as stresses at the distal end are the result of waves travelling from the proximal end that are far lower in intensity than the compaction wave.

The only difference the higher crushing speed makes is the higher amplitudes of the oscillations in the stresses. This is believed to be due to the effects of a mixture of the transmission of the stress oscillation in the compacted region at the proximal end and the local separations between nodes and the support at the distal end. A close examination of the responses at the distal end reveals that some (all, sometimes) nodes get separated from the support at some point of time. Dynamically, such separation results in local unloading and hence generates release waves which complicate the whole crushing process, but this is beyond the scope of the present paper.

The stress–compression curves show a general increase in the length of the plateau (with respect to δ) as the crushing speed increases. The stress at the proximal end is approximately equal to the stress in the compacted region. Increase in this compressive stress evidently results in higher densification strain in the compacted region and produces a longer plateau. The relationship between the densification strain and the crushing velocity is given in Fig. 8. The dynamic densification strain increases as crushing velocity increases and asymptotes to a limit when a steady-shock front is generated in the honeycombs, which is 15% higher than the quasi-static one. In the shock theory based on *R-P-P-L* idealisation [1,2], the locking strain, i.e. densification strain, is assumed constant

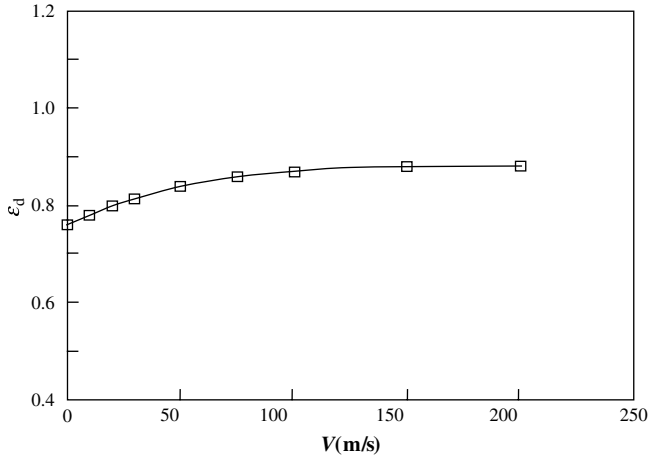

Fig. 8. Densification strains of the honeycomb under different crushing velocities (cells compressed in X_1 direction, $\bar{\rho} = 0.1$).

at the quasi-static value. The present finding implies a modification to the shock theory is required and is addressed later in this paper.

5.2. Distribution of compressive strain and thickness of shock

Distributions of compressive strain as defined in Section 4 can be obtained from the output of the ABAQUS analyses. Fig. 9 shows such distributions in the honeycomb for two crushing speeds, viz.

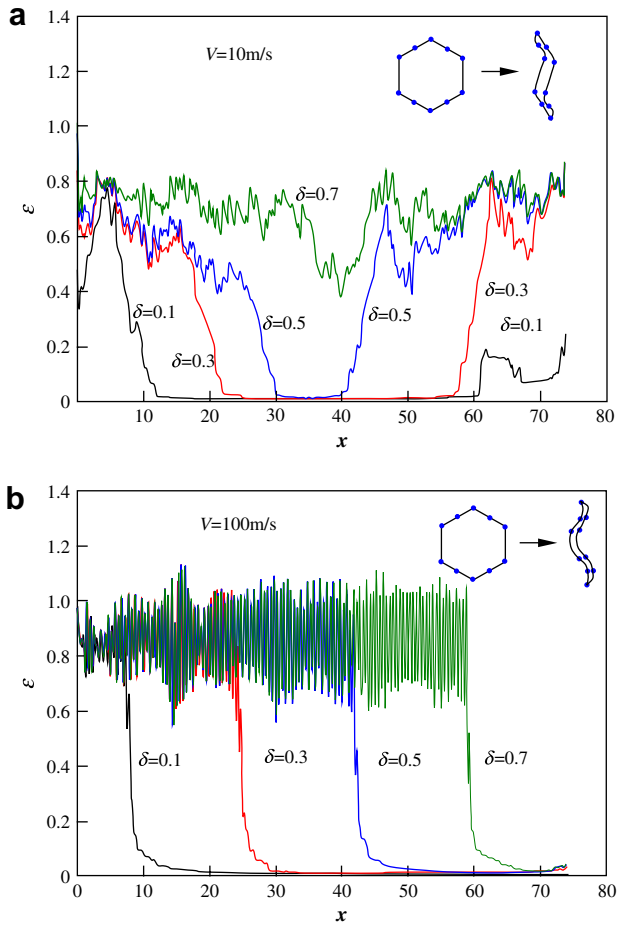

Fig. 9. Distribution of compressive strain (cells compressed in X_1 direction, $\bar{\rho} = 0.1$).

10 and 100 m/s over a range of crushing displacement, δ, of 0.1, 0.3, 0.5 and 0.7. There are 74 rows of cells in the honeycomb along the loading direction. The x-coordinate in Fig. 9 has been normalised with respect to the cell length so that the normalised x value is therefore directly related to the cell number.

Under low speed compression ($V = 10$ m/s), the strain reaches a high value (0.7–0.78) around the two ends first. The high compressive strains from both ends propagate towards the middle of the honeycomb as the crushing displacement δ increases. The strain around the distal end does not rise immediately to the densification strain (about 0.78), as shown in Fig. 9a for $\delta = 0.1$. This is because strains are calculated from the cross-sectional displacements and the crushing bands are not parallel to the cross-section but inclined somewhat as shown in Figs. 3 and 4, i.e. the "X" and "V" shaped crushing bands. However, as crushed zones build up, the densification strain is achieved gradually. Most of the cells crushed take shapes similar to that shown in the inset to Fig. 9a at this crushing speed, which suggests a significant shear deformation as a result of local buckling of the cell walls.

At high crushing speed, the distribution of compressive strain is localised at the proximal end as shown in Fig. 9b. The crushed zone grows as the process proceeds. Greater compaction is obtained in the crushed zones of the honeycomb than at low speed compression. Once the cells are crushed, the strain remains approximately unchanged as the rest of the honeycomb is compressed. The fluctuations in the strain distribution in the compacted region reflect the non-uniform local compression within a cell. At this crushing speed, most cells collapse in a pattern similar to that depicted in the inset to Fig. 9b. The characteristics of this pattern differ from those produced at low speed. The symmetrical appearance suggests a more stable process of deformation instead of unstable buckling, the resistance from the effects of inertia providing a stabilising effect against buckling. Due to the cellular nature of the honeycomb, the local deformation within a cell is very irregular and non-uniform after cell collapse. Cross-sections originally distributed uniformly within a given row of cells deform irregularly, resulting in a big variation in the relative displacements between them. The neighbouring cross-sections may even penetrate into each other after cell collapse. The strain definition based on the average cross-sectional displacement used in the present paper therefore fluctuate considerably, leading to strain values exceeding 1, occasionally. However, if the strain was calculated over the length of one row of cells instead of from the two neighbouring cross-sections, the strain thus obtained in the crushed zone would be much more uniform and rise to the densification strain straightaway.

Of particular interest at high crushing speeds is the breadth of the band of cells which comprise the front of the deformation zone, in which cells are undergoing collapse. In the compressive strain distribution curves, the compressive strain increases rapidly from a magnitude of approximately 0.1 to the densification strain across this band, see Fig. 9b. The width of this band is much narrower than that produced by low compression rates. Fig. 10 shows the distribution of the compressive strain around the collapsing band at different compression speeds as the crushing front passes the same region of the honeycomb (cells from row 38 to row 48). At $V = 50$ m/s, the compressive strain increases to densification level gradually across about three to four cells. Once the crushing speed exceeds 75 m/s, the compression strain exhibits virtually a step change across the length of a single cell from $\varepsilon_0 \approx 0.1$ to the densification strain, as depicted by the broken lines. The thickness of this collapsing band remains almost unchanged as the crushing front propagates and as the crushing speed increases to even higher values, e.g. 100 and 200 m/s.

To understand the variations in the thickness of the crushing band better, a parametric study was conducted on honeycombs of different relative densities. The distributions of the compressive strain around the crushing band for honeycombs of relative densities of 0.05 and 0.2 are given in Fig. 11a and b, respectively, as opposed to 0.1 as discussed above. They clearly show a thickness of approximately one cell diameter wherein the magnitude of the change in strain is greater than approximately 85% of the densification strain (i.e. the thickness of the crushing bands is about one

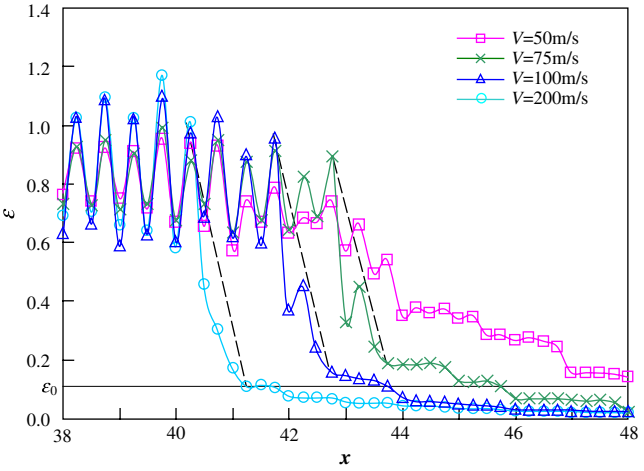

Fig. 10. Strain distribution across the crushing front (cells compressed in X_1 direction, $\bar{\rho} = 0.1$, $\delta = 0.5$).

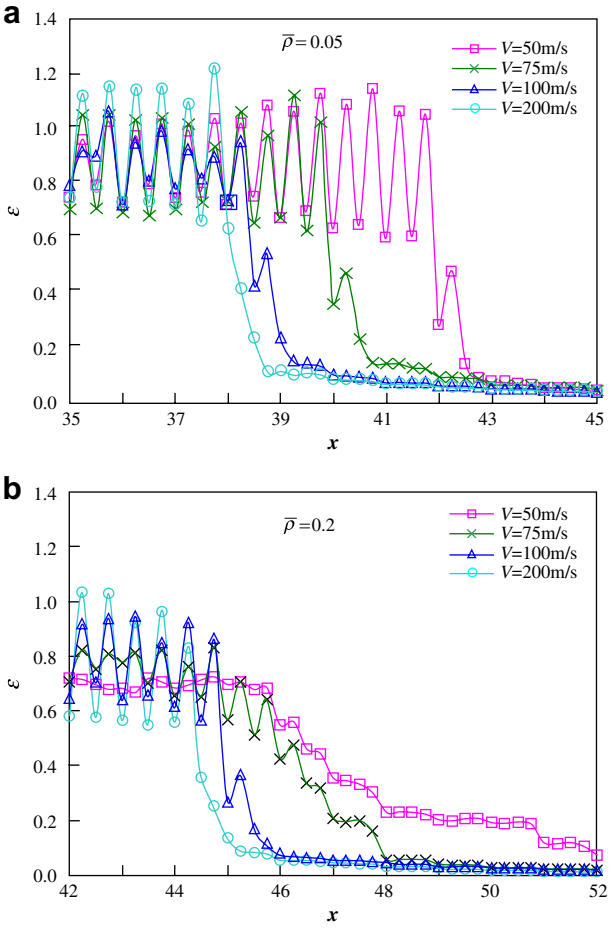

Fig. 11. Strain distribution across the crushing front in honeycombs with different relative density (cells compressed in X_1 direction, $\delta = 0.5$).

single cell diameter) once the crushing velocity exceeds the steady-shock velocity V_s. In general, the higher the relative density of the honeycomb, the higher the steady-shock velocity V_s. This dependency is represented by Eq. (5), wherein the quasi-static crush strength σ_0 scales with the square of the density ρ whereas the densification strain ε_d is only weakly dependent on density.

When the honeycomb is crushed in the X_2 direction, refer to Fig. 2b, the compressive strain distributions obtained under different crushing speeds are given in Fig. 12. The pattern of deformation differs somewhat from the previous ones, as depicted in the inset. As the inclined edges tend to displace to the interior of the cell as the cell collapses, according to our definition, the compressive strain obtained may well exceed unity. However, the average strain in the crushed zone is still around 0.87, the level for the densification strain as in the case of cell compression in the X_1 direction. The steady-shock crushing speed which corresponds to a step increase in the compression strain is around 75 m/s. The crushing band thickness is also about the length of a single cell. For high velocity compression, the global behaviour of the honeycomb is approximately the same as when it is loaded in the X_1 direction.

All the above results show that there exists a characteristic parameter pertaining to the propagating shock front at supercritical velocities ($V > V_s$), the thickness of the crushing band. It is dominated by the construction of the honeycomb and almost independent of the crushing velocity and relative density, provided the compression velocity is supercritical, although the critical crushing speed for sustaining shock-type behaviour varies with the relative density. This thickness of the crushing band can be considered effectively as the thickness of the shock. Approximately 90% of the compression occurs within this band with a thickness around one cell diameter. It can therefore be postulated that a shock forms when the length of the crushing band reduces to one cell size and this takes place as the crushing speed increases to and beyond the critical crushing speed. It was also conjectured from experiments by Radford et al. [22] that shocks have a thickness comparable to the cell size in metal foams.

5.3. Sectional velocity distributions

To reinforce the understanding of shock thickness as discussed above, distributions of the material 'particle' velocity, more precisely sectional velocity, in the honeycomb have been obtained and are presented in Fig. 13 at a range of different global compression levels when the honeycomb is crushed at a speed of 100 m/s which

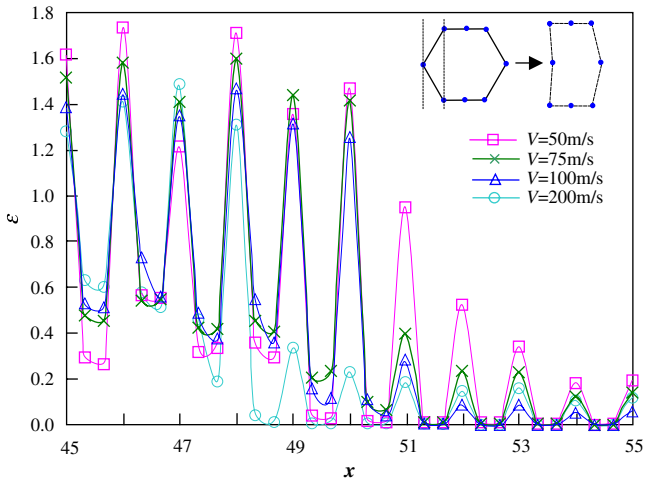

Fig. 12. Strain distribution across the crushing front with cells compressed in X_2 direction ($\bar{\rho} = 0.1$, $\delta = 0.5$).

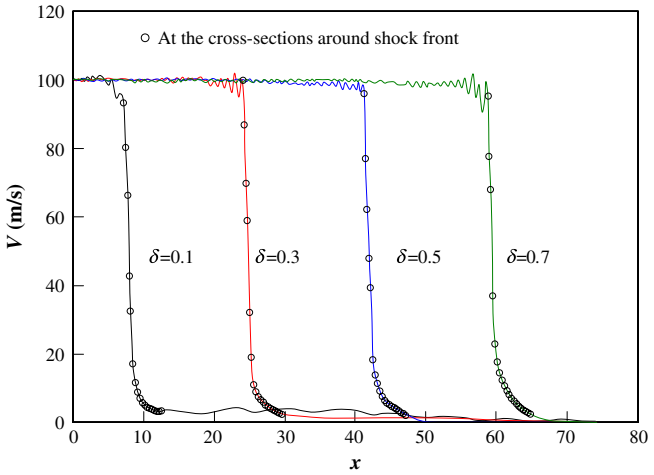

Fig. 13. Distribution of the sectional velocity (cells compressed in X_1 direction, $\bar{\rho} = 0.1$, $V = 100$ m/s).

is supercritical ($V > V_s$) for this particular honeycomb. Similar to the strain, there is a step change in the sectional velocities ahead of and behind the shock front. The sectional velocity in the shock-disturbed region behind the shock front levels to the crushing speed after a number of slight oscillations. The velocity rises to the imposed boundary velocity from a very low value and 80% of this change in velocity takes place over a length of about one cell diameter (where a complete cell covers five cross-sections). The majority of the remaining 20% change in particle velocity occurs over the two layers of cells that are immediately ahead of the major transition zone. This reinforces the conclusion made in the previous Section that the thickness of the shock is about one cell diameter. Immediately ahead of the shock front, the sectional velocity is not equal to zero as assumed in the *R-P-P-L* shock theory. It takes about 5–10 cells to achieve that in a smooth manner. The transition to the final velocity is complex but is probably related to the way elastic bending waves in the cell walls disperse. This transition zone serves as the precursor of the incoming shock wave. This observation indicates that there are two compression stages during the cell collapse process. Cross-sections are first disturbed to achieve a low velocity of about 5 m/s. As the shock front arrives, cross-sections are accelerated to the crushing speed in a very short time period (about one cell length divided by the shock propagation velocity).

In the early stages of deformation, e.g. at $\delta = 0.1$ and 0.3, over a large distance ahead of the shock front, there is a small sectional velocity which disappears as the crushing progresses. This phenomenon can be explained as follows. In the early stages of compression, local (elastic and even plastic) deformation occurs in the cells at the distal end as well. As a result, the remaining part of the honeycomb translates in a more or less rigid body sense and hence a fairly uniform small velocity is found in the part of the honeycomb ahead of the shock front but away from the distal end. For larger displacements at the proximal end, there is insufficient length outside the compacted region to have an undeformed section moving with an almost constant velocity.

5.4. Stress distributions in the honeycomb

The stresses at the proximal and distal ends were obtained directly from the reaction force available in ABAQUS. These are experimentally measurable. However, it would be difficult, if not impossible, to measure stresses experimentally within the honeycomb. In order to understand the crushing process and to relate it to the stresses in the honeycomb, efforts have therefore been made to

find the stress distribution in the honeycomb numerically. The stress to be calculated represents that on a cross-section and the calculation has been performed in a section-wise manner. At each section, the accelerations at all the nodes on one side of the section have been extracted from the ABAQUS output. The mass of the honeycomb walls has been distributed to the nodes according to a lumped mass idealisation as employed conventionally in dynamic analyses, especially involving an explicit algorithm, as is the case of present analysis. The internal force at a given cross-section can then be obtained by applying the equation of motion to the material on that side of the section which is considered as a free body. The resultant is the sum of the reaction at the end, proximal or distal, and the products of all nodal masses and respective accelerations in the free body. The sectional stress is obtained as the force divided by the nominal cross-section area of the honeycomb.

Fig. 14 shows the stress distributions within the honeycomb thus obtained at the time when the entire honeycomb was crushed to an overall compression level $\delta = 0.5$. As expected, there is little stress variation over the length of the honeycomb at low crushing velocity. Increasing the crushing velocity gradually results in a non-uniform stress distribution in the honeycomb. The honeycomb in the compacted region is at a raised stress level and the stresses in the honeycomb on the other side remain at, more or less, the quasi-static crushing stress. The difference between the stresses in these two regions becomes more pronounced as the crushing velocity increases. The distributions of stress also suggest the existence of a shock when the crushing speed is sufficiently high ($V > V_s$).

Apart from an almost distinct step change (shock front) in the stress distribution when the honeycomb is subjected to compression at a supercritical speed, there are secondary variations in the two regions, i.e. behind and ahead of the shock front. There appears to be more variation behind the shock front than in the region ahead, reflecting the level of complication in the travelling stress waves in these two regions. It can also be seen in Fig. 14 that the higher the crushing velocity, the higher the magnitudes of the fluctuations. The average of the stress in the regions behind and ahead of the shock front approximate the two stress levels in the honeycomb predicted in the *R-P-P-L* shock theory.

5.5. Energy absorption

In order to estimate the effects of increased crushing speed on the energy absorption capacity of the honeycomb, the dissipated plastic energies in the whole model over a range of crushing speeds have been calculated and presented as functions of the overall

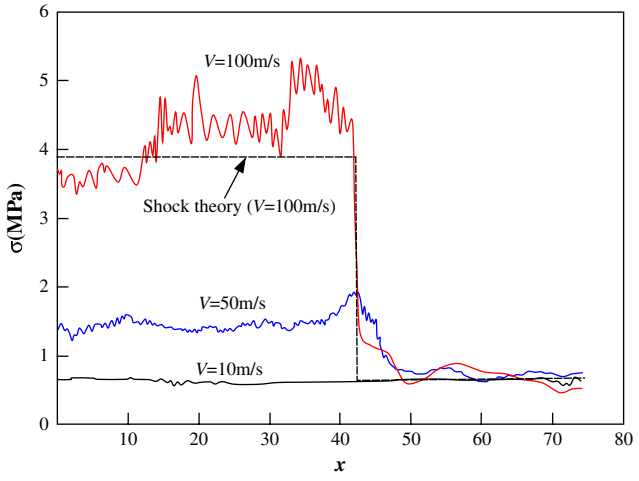

Fig. 14. Distribution of compressive stress in the honeycomb (cells compressed in X_1 direction, $\bar{\rho} = 0.1$, $\delta = 0.5$).

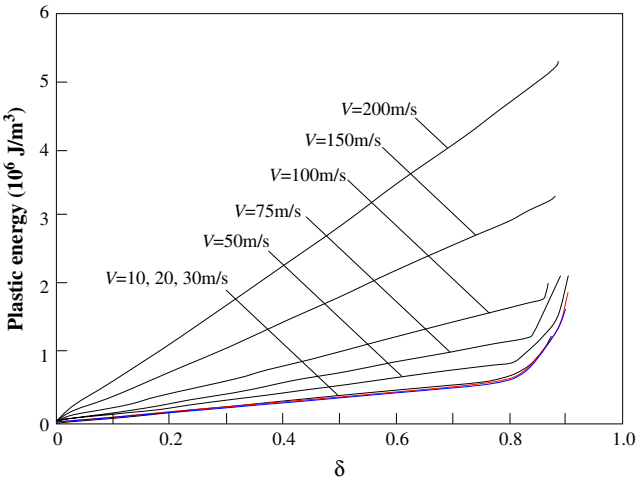

Fig. 15. Effect of compression velocity on energy absorption (cells compressed in X_1 direction, $\bar{\rho} = 0.1$).

compression level δ, as shown in Fig. 15, where the energies have been normalised with respect to the volume of the whole honeycomb. The energies at all different crushing velocities increase almost linearly with the overall compression up to the point of global densification. At lower crushing velocities, little effects of crushing velocity can be seen on the plastic energy absorbed as expected. However, higher compression velocities result in a significant enhancement of the plastic energy. The capacity of plastic energy dissipation increases as the compression velocity is raised. Plastic energy dissipation is increased by about 50%, 300% and 800% when the honeycombs are compressed to the same level at crushing velocities of 50, 100 and 200 m/s, respectively, compared with that under quasi-static loading. Additional FE analysis on a small sample with each edge of cell walls modelled with 10 elements shows that this is mainly due to the increased local plastic bending and axial compression strains in the inclined cell walls around their ends. At low crushing speeds, the plastic energy is dominated by bending of cell walls as a result of buckling and post-buckling deformation. In problems involving high crushing speed, the buckling and post-buckling deformation is retarded by the sideway inertial forces, which leaves time for extensive localised bending and axially compression to occur around the ends of the inclined edges at high impact velocity before the global bending mechanism is established and dominates. For cell collapse at an impact velocity of 100 m/s, the curvature and membrane compression strain in the element at the ends may be as high as 2 times and 20 times of the corresponding values under the quasi-static loading, respectively.

Fig. 16 shows the history of the kinetic and plastic energy in the middle row (35th) of cells from the proximal end as functions of overall compression. The step changes in the kinetic energy and plastic energy occur when the shock passes this row of cells when the honeycombs are compressed at high speed. This suggests that most of the plastic energy absorption by this row of cells take place when the shock front passes through this row of cells.

6. Discussion – validation of one-dimensional *R-P-P-L* shock theory

Fig. 17a and b shows the comparisons between the FE analysis and *R-P-P-L* shock theory Eqs. (1) and (2), in terms of predicted crushing plateau stress and energy absorption as functions of the compression velocity, respectively. The comparison is generally good. In particular, the large increase of plastic work with increased impact velocity due to the presence of the shock is verified by the

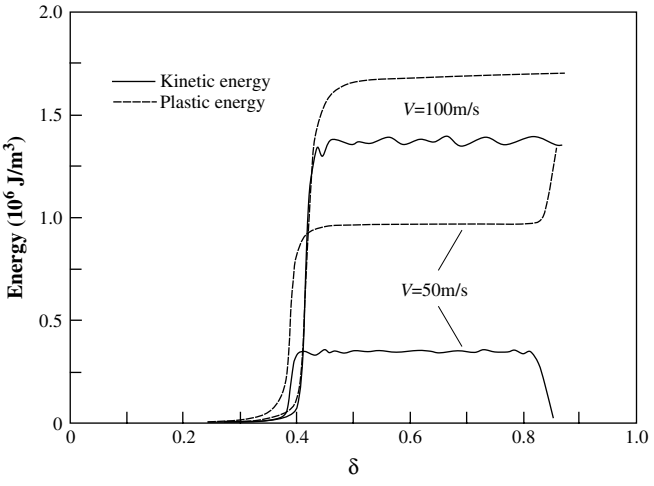

Fig. 16. Energy history at the 35th row of cells (cells compressed in X_1 direction, $\bar{\rho} = 0.1$).

FE model. The reason for this agreement is presumably the use of momentum conservation in the two solution schemes with a consequent absorption of energy. The mechanism of energy absorption relies on the particular deformation/dissipation mechanisms allowed in the models. In this case, the additional energy absorbed is ascribed to plastic deformation. Further discussion of this phenomenon will be made in a future publication.

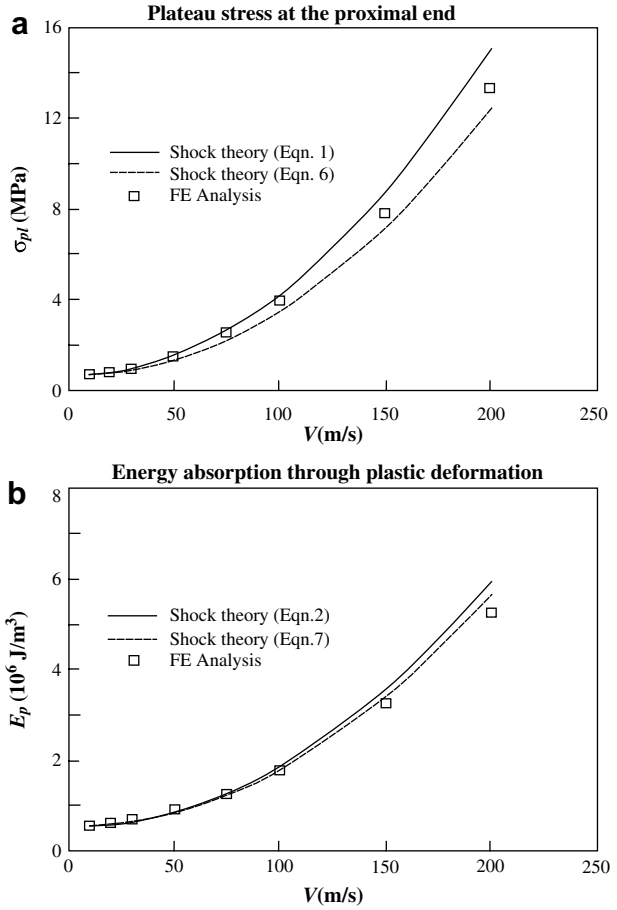

Fig. 17. Comparisons between FE analysis and shock theory (cells compressed in X_1 direction, $\bar{\rho} = 0.1$).

For a honeycomb of relative density 0.1, equivalent to a density of the cellular material $\rho = 270\ \mathrm{kg\,m^{-3}}$, the finite element simulation predicts a quasi-static crushing strength $\sigma_0 = 0.7$ MPa and a quasi-static densification strain $\varepsilon_d = 0.76$. When these values are used in *R-P-P-L* shock theory Eqs. (1) and (2) which assumes ε_d constant at the quasi-static loading value, it predicts results in reasonable agreement with the FE prediction with a degree of overestimation, which could amount to about 15–20% above the FE prediction when the compression velocity is high.

The shock theory predictions are strongly dependent on the material model used to approximate the cellular material. Ideally for a continuum, an equation of state that relates shock speed with particle velocity would be used together with the Rankine–Hugoniot jump conditions to relate changes in state across the shock. A more general form of Eqs. (1) and (2) is

$$\sigma = \sigma_A + \frac{\rho[V]^2}{[\varepsilon]} \tag{6}$$

$$E_p = \sigma_A[\varepsilon] + \frac{1}{2}\rho[V]^2 \tag{7}$$

where σ_A is the stress just ahead of the shock and [ ] denotes a change in the value across the shock (see Ref. [15]), and E_p is the specific plastic energy dissipation through shock compression of the material. Using Eqs. (6) and (7) it is possible to produce a second shock theory prediction that takes account of more realistic states on either side of the shock. Here, it is assumed that $\sigma_A = \sigma_0$, $[V] = V - V_w$ and $[\varepsilon] = \varepsilon_d(V) - \varepsilon_w$, where $\varepsilon_d(V)$ is the densification strain defined as a function of the velocity of the striker according to Fig. 8. With these conditions, Eqs. (6) and (7) agree with the FE predictions to within ±7.5% for the range of velocities considered. These conditions are again somewhat idealised as the states on either side of the shock are constantly changing as a result of reflections with the boundaries and the degree of deformation within the collapsing cells. Furthermore, it is difficult to justify the use of quasi-static collapse conditions to define the material state ahead of the shock. Nonetheless they illustrate the sensitivity of the shock theory to the material model that is employed.

Both Eqs. (1) and (6) agree well with the FE model in the low velocity régime ($V < 50$ m/s for the present case) even though a sharp shock front is not actually present. In fact, Eq. (5) predicts a steady-shock velocity V_s of 66 m/s. This is consistent with the observation from the FE simulation as indicated in Fig. 10 where the critical velocity V_s is between 50 m/s and 75 m/s to produces a one cell size thick crushing front.

Ideally, one could use a series of states within fully collapsed, partially collapsed and relatively undeformed portions of the FE model to construct a Hugoniot and Rayleigh lines to enable a fuller description of the shock deformation of the honeycomb for impact speeds greater than V_s. This has proved difficult due to fluctuations in stresses and strains in the FE predictions. However, certain features of the predictions of the FE model have been consistent and are worth noting. Before the shock front reaches a cell, the strain of the cell has already been raised to a level around $\varepsilon_0 = 0.1$ as a kind of precursor, as can be seen in Fig. 10. The FE results suggest that this precursor strain ε_0 is primarily plastic while the elastic component is negligible. The stresses associated with this precursor are greater than σ_0 (see Fig. 14) and so the state of the material ahead of the shock cannot be associated with a point on the quasi-static stress–strain curve.

7. Conclusions

The dynamic crushing of honeycomb has been simulated using finite elements. Cell collapse generally initiates at the distal and

proximal ends when crushed at low crushing speed. Subsequently the deformation spreads to the centre of the honeycomb through the cumulative multiplication of discrete bands. As the crushing velocity increases beyond a critical value associated with steady-shock velocity, cell collapse starts at the proximal end and propagates progressively towards the distal end in a shock-like manner. This critical crushing velocity varies with the relative density of the honeycomb which is well represented by Eq. (5).

There is a characteristic shock thickness associated with the propagating shock front at supercritical velocities, which is around one cell diameter. This thickness is almost independent of the crushing velocity (provided it is supercritical) and relative density of the honeycomb, although the magnitude of the critical compression velocity for the formation of shock increases as the relative density of the honeycomb increases.

The results from the FE analysis have been used to examine the assumptions made in the one-dimensional shock model based upon a rigid-perfectly plastic-locking idealisation for the stress–strain curve. It has been demonstrated that the crushing stress and the plastic energy dissipation density are both enhanced by increased crushing velocity. Once the crushing velocity is high enough to form a shock in the honeycomb, both the crushing stress and the plastic energy are related to the crushing velocity by a square law. Densification strain also increases as crushing velocity increases and asymptotes to a limit once shock front forms. The classical one-dimensional *R-P-P-L* shock model tends to overestimate the crushing stress and the energy absorption slightly. An effort has been made to illustrate the sensitivity of the shock theory to the material model that is employed.

Acknowledgements

This work is funded by the EPSRC (UK) under grant number GR-R26542.

References

[1] Reid SR, Peng C. Dynamic uniaxial crushing of wood. Int J Impact Eng 1997;19:531–70.
[2] Tan PJ, Reid SR, Harrigan JJ, Zou Z, Li S. Dynamic compressive strength properties of aluminium foams. Part II – shock theory and comparison with experimental data and numerical models. J Mech Phys Solids 2005;53:2206–30.
[3] Gibson LJ, Ashby MF. Cellular solids, structures and properties. 2nd ed. Cambridge, UK: Cambridge University Press; 1997.
[4] Reid SR, Reddy TY, Peng C. Dynamic compression of cellular structures and materials. In: Jones N, Wierzbicki T, editors. Structural crashworthiness and failure. London: Elsevier Applied Science Publishers; 1993. p. 295–340.
[5] Zhao H, Gary G. Crushing behaviour of aluminium honeycombs under impact loadings. Int J Impact Eng 1998;21:827–36.
[6] Tan PJ, Harrigan JJ, Reid SR. Inertia effects in uniaxial dynamic compression of a closed cell aluminium alloy foam. Mat Sci Tech 2002;18:480–8.
[7] Tan PJ, Reid SR, Harrigan JJ, Zou Z, Li S. Dynamic compressive strength properties of aluminium foams. Part I – experimental data and observations. J Mech Phys Solids 2005;53:2174–205.
[8] Hönig A, Stronge WJ. In-plane dynamic crushing of honeycomb. Part I, crush band initiation and wave trapping. Int J Mech Sci 2002;44:1665–96.
[9] Hönig A, Stronge WJ. In-plane dynamic crushing of honeycomb. Part II, application to impact. Int J Mech Sci 2002;44:1697–714.
[10] Reid SR, Bell WW, Barr R. Structural plastic model for one-dimensional ring systems. Int J Impact Eng 1983;1:185–91.
[11] Hanssen AG, Enstock L, Langseth M. Close-range blast loading of aluminium foam panels. Int J Impact Eng 2002;27:593–618.
[12] Zhao H, Elnasri I, Abdennadher S. An experimental study on the behaviour under impact loading of metallic cellular materials. Int J Mech Sci 2005;47:757–74.
[13] Lopatnikov SL, Gama BA, Haque MJ, Krauthauser C, Gillespie JW, Guden M, et al. Dynamics of metal foam deformation during Taylor cylinder – Hopkinson bar impact experiment. Compos Struct 2003;61:61–71.
[14] Lopatnikov SL, Gama BA, Haque MJ, Krauthauser C, Gillespie JW. High velocity plate impact of metal foams. Int J Impact Eng 2004;30:421–45.
[15] Harrigan JJ, Reid SR, Tan PJ, Reddy TY. High rate crushing of wood along the grain. Int J Mech Sci 2005;47:521–44.
[16] Ruan D, Lu G, Wang B, Yu TX. In-plane dynamic crushing of honeycombs – finite element study. Int J Impact Eng 2003;28:161–82.
[17] Zheng Z, Yu J, Li J. Dynamic crushing of 2D cellular structures: a finite element study. Int J Impact Eng 2005;32:650–64.
[18] Hibbitt, Karlsson & Sorensen, Inc.. ABAQUS explicit user's manual, Version 6.3. Providence Rhode Island: HKS; 2002.
[19] Calladine CR, English RW. Strain-rate and inertia effects in the collapse of two types of energy-absorbing structure. Int J Mech Sci 1984;26:689–701.
[20] Su XY, Yu TX, Reid SR. Inertia-sensitive impact energy-absorbing structures. Part I: effects of inertia and elasticity. Int J Impact Eng 1995;4:651–72.
[21] Zou Z, Tan PJ, Reid SR, Li S, Harrigan JJ. Dynamic crushing of a one dimensional chain of Type II structures. Int J Impact Eng 2007;34:303–28.
[22] Radford DD, Deshpande VS, Fleck NA. The use of metal foam projectiles to simulate shock loading on a structure. Int J Impact Eng 2005;31:1152–71.